Inorg. Chem. **2009**, *48*, 3934−3942

Direct Deconvolution of Two-State Pump-Probe X-ray Absorption Spectra and the Structural Changes in a 100 ps Transient of Ni(II)-tetramesitylporphyrin

S. Della-Longa,[*,†,‡] L. X. Chen,[§,||] P. Frank,[⊥,#] K. Hayakawa,[‡,▽] K. Hatada,[‡] and M. Benfatto[*,‡]

Dipartimento Medicina Sperimentale, Università dell' Aquila, 67100 L'Aquila, Italy, Laboratori Nazionali di Frascati, INFN, CP13, I-00044 Frascati, Italy, Chemical Sciences and Engineering Division, Argonne National Laboratory, 9700 South Cass Avenue, Argonne, Illinois 60439, Department of Chemistry, Northwestern University, Evanston, Illinois 60208, Department of Chemistry, Stanford University, Stanford, California 94305-5080, Stanford Synchrotron Radiation Laboratory, SLAC, Stanford University, Stanford, California 94309, and Museo storico della Fisica e Centro Studi e Ricerche "Enrico Fermi", via Panisperna 89A, 00184 Roma, Italy

Received May 16, 2008

Full multiple scattering (FMS) Minuit XANES (MXAN) has been combined with laser pump-probe K-edge X-ray absorption spectroscopy (XAS) to determine the structure of photoexcited Ni(II)tetramesitylporphyrin, Ni(II)TMP, in dilute toluene solution. It is shown that an excellent simulation of the XANES spectrum is obtained, excluding the lowest-energy bound-state transitions. In ground-state Ni(II)TMP, the first-shell and second-shell distances are, respectively, d(Ni−N) = (1.93 ± 0.02) Å and d(Ni−C) = (2.94 ± 0.03) Å, in agreement with a previous EXAFS result.[1] The time-resolved XANES difference spectrum was obtained[1] from the spectra of Ni(II)TMP in its photoexcited T_1 state and its ground state, S_0. The XANES difference spectrum has been analyzed to obtain both the structure and the fraction of the T_1 state. If the T_1 fraction is kept fixed at the value (0.37 ± 0.10) determined by optical transient spectroscopy, a 0.07 Å elongation of the Ni−N and Ni−C distances [d(Ni−N) and d(Ni−C)] is found, in agreement with the EXAFS result. However, an evaluation of both the distance elongation and the T_1 fraction can also be obtained using XANES data only. According to experimental evidence, and MXAN simulations, the T_1 fraction is (0.60 ± 0.15) with d(Ni−N) = (1.98 ± 0.03) Å (0.05 Å elongation). The overall uncertainty of these results depends on the statistical correlation between the distances and T_1 fraction, and the chemical shift of the ionization energy because of subtle changes of metal charge between the T_1 and S_0 states. The T_1 excited-state structure results, independently obtained without the excited-state fraction from optical transient spectroscopy, are still in agreement with previous EXAFS investigations. Thus, full multiple scattering theory applied through the MXAN formalism can be used to provide structural information, not only on the ground-state molecules but also on very short-lived excited states through differential analysis applied to transient photoexcited species from time-resolved experiments.

Introduction

X-ray Absorption Spectroscopy (XAS) is a powerful tool for determining both electronic and structural information about systems ranging from biological molecules to condensed matters. On one hand, X-ray Absorption Near-Edge Structure (XANES) provides details about the electronic structure of the absorbing atom, i.e., orbital occupancy, oxidation state, ligand field strength and the coordination symmetry of its valence states. On the other hand, coordination numbers and bond distances around a specific atom can be determined from the Extended X-ray Absorption Fine Structure (EXAFS). Hence, XAS can be particularly useful in the search for relationships between electronic states and structural geometry for metal centers in chemistry and biology, as well as materials sciences.

* To whom correspondence should be addressed. E-mail: dlonga@caspur.it (S.D.-L.), maurizio.benfatto@lnf.infn.it (M.F.). Phone: +39-0862-433568 (S.D.-L.), +39-06-94032884 (M.F.). Fax: +39 −0862-433523 (S.D.-L.), +39-06-94032427 (M.F.).
† Università dell' Aquila.
‡ Laboratori Nazionali di Frascati, INFN.
§ Argonne National Laboratory.
|| Northwestern University.
⊥ Department of Chemistry, Stanford University.
Stanford Synchrotron Radiation Laboratory, SLAC, Stanford University.
▽ Museo storico della Fisica e Centro Studi e Ricerche "Enrico Fermi".

10.1021/ic8008943 CCC: $40.75
Published on Web 03/27/2009

In recent years, an increasing number of studies on the structure of transient photoexcited states have used pump-probe XAS spectroscopy, in which the system is excited by an ultrashort laser pulse and probed by a time-delayed X-ray pulse.[1−12] In this way it is possible to obtain both electronic and structural changes due to the photoexcitation. Metalloporphyrins are versatile functional groups in various photochemical reactions, enabling the intra- and intermolecular energy or electron redistribution that can trigger photochemical processes. However, details of the electronic configuration and molecular geometry of the photoexcited state are not completely understood from previous steady-state structural determination methods, or indirect structural methods such as optical transient absorption spectroscopy.

Several years ago Benfatto and Della Longa proposed[13] a fitting procedure, MXAN (Minuit XANES) based on a full multiple scattering (MS) theory, which could extract local structural information around the absorbing atom from experimental XANES data. Since then, the MXAN method has been successfully used for analyses of many known and unknown systems, yielding structural geometries and metrics comparable to X-ray diffraction and/or EXAFS results.[14−18]

Recently the MXAN method was modified to enable the extraction of structural information from a difference spectrum reflecting the sudden change from a molecular ground state to an excited state following an external perturbation, such as a laser pulse. The importance of differential XAS spectra for revealing very small structural and electronic changes in a sample has been emphasized in both EXAFS and XANES regions in recent years.[19−21] The methodological validity of differential XAS depends critically on a perfect energy stability during the experiment, and a proper accounting of any shift in the ionization energy.[20] However, the advantages of this method include an enhanced sensitivity of curve fitting and the reduced influence of possible systematic errors in calculations stemming from the approximations used in the theoretical approach.

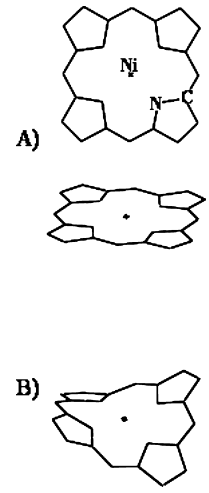

Figure 1. Two Ni-porphyrin core structures used in calculating the XANES fits and for testing twisting effects: (A) perfectly planar, and; (B) saddle-shaped.

In this paper we present an analysis of the ground and photoexcited state Ni K-edge XAS spectra of Ni(II)tetramesitylporphyrin (NiTMP), in a dilute toluene solution, depicted in Figure 1A. The excited-state XANES spectrum was obtained at nominally 100 ps after the Q-band laser pulse excitation at 527 nm (note: the accuracy of the delay time is limited by the response time of the detector at <100 ps). The experimental data, shown in Figure 2, were obtained from Chen et al.[1] who reported an analysis of EXAFS spectra for the S_0 and T_1 states. These workers reconstructed the T_1 state XAS spectrum from the 100 ps spectrum by subtracting the fractional remaining S_0 state XAS, which was independently determined using optical transient absorption spectroscopy.

We have shown that it is possible to extract the structure of the S_0 and T_1 states from analysis of the "laser-on minus laser-off" difference XANES spectra without the additional information on the T_1 state fraction. Successful treatment of metalloporphyrin systems will allow extension of the MXAN method to K-edge photoinduced transient difference XANES spectra of transition metal complexes with low coordination symmetry, which normally have a richly featured rising edge region. In this report, the MXAN method is shown to successfully treat metalloporphyrins, with an excellent simulation and local structural recovery. The results also demonstrate that the differential XANES spectral analysis

(1) Chen, L. X.; Zhang, X.; Wasinger, E. C.; Attenkofer, K.; Jennings, G.; Muresan, A. Z.; Lindsey, J. S. *J. Am. Chem. Soc.* **2007**, *129*, 9616–9618.
(2) Chen, L. X.; Jager, W. J. H.; Jennings, G.; Gosztola, D. J.; Munkholm, A.; Hessler, J. P. *Science* **2001**, *292*, 262–264.
(3) Chen, L. X.; Jennings, G.; Liu, T.; Gosztola, D. J.; Hessler, J. P.; Scaltrito, D. V.; Meyer, G. J. *J. Am. Chem. Soc.* **2002a**, *124*, 10861–10867.
(4) Chen, L. X. *Faraday Discuss.* **2002b**, *122*, 315–329.
(5) Chen, L. X.; Shaw, G. B.; Novozhilova, I.; Liu, T.; Jennings, G.; Attenkofer, K.; Meyer, G. J.; Coppens, P. *J. Am. Chem. Soc.* **2003**, *125*, 7022–7034.
(6) Saes, M.; Bressler, C.; Abela, R.; Grolimund, D.; Johnson, S. L.; Heimann, P. A.; Chergui, M. *Phys. Rev. Lett.* **2003**, *90* (047403), 1–4.
(7) Bressler, C.; Chergui, M. *Chem. Rev.* **2004**, *104*, 1781–1812.
(8) Chen, L. X. *Angew. Chem., Int. Ed.* **2004**, *43*, 2886–2905.
(9) Chen, L. X.; Shaw, G. B.; Liu, T.; Jennings, G.; Attenkofer, K. *Chem. Phys.* **2004**, *299*, 215–223.
(10) Saes, M.; Bressler, C.; van Mourik, F.; Gawelda, W.; Kaiser, M.; Chergui, M.; Bressler, C.; Grolimund, D.; Abela, R.; Glover, T. E.; Heimann, P. A.; Schoenlein, R. W.; Johnson, S. L.; Lindenberg, A. M.; Falcone, R. W. *Rev. Sci. Instrum.* **2004**, *75*, 24–30.
(11) Chen, L. X. *Annu. Rev. Phys. Chem.* **2005**, *56*, 221–254.
(12) Gawelda, W.; Pham, V. T.; Benfatto, M.; Zaushitsyn, Y.; Kaiser, M.; Grolimund, D.; Johnson, S. L.; Abela, R.; Hauser, A.; Bressler, C.; Chergui, M. *Phys. Rev. Lett.* **2007**, *98* (057401), 1–4.
(13) Benfatto, M.; Della Longa, S. *J. Synchrotron Radiat.* **2001**, *8* (4), 1087–1094.
(14) Benfatto, M.; D'Angelo, P.; Della Longa, S.; Pavel, N. V. *Phys. Rev. B* **2002**, *65* (174205), 1–5.
(15) D'Angelo, P.; Benfatto, M.; Della Longa, S.; Pavel, N. V. *Phys. Rev. B* **2002**, *66* (6), 64209–64215.
(16) Hayakawa, K.; Hatada, K.; D'Angelo, P.; Della Longa, S.; Natoli, C. R.; Benfatto, M. *J. Am. Chem. Soc.* **2004**, *126* (47), 15618–15623.
(17) Frank, P.; Benfatto, M.; Szilagyi, R. K.; D'Angelo, P.; Della Longa, S.; Hodgson, K. O. *Inorg. Chem.* **2005**, *44* (6), 1922–1933.
(18) Arcovito, A.; Benfatto, M.; Cianci, M.; Hasnain, S. S.; Nienhaus, K.; Nienhaus, G. U.; Savino, C.; Strange, R. W.; Vallone, B.; Della Longa, S. *Proc. Natl. Acad. Sci. U.S.A.* **2007**, *104* (15), 6211–6216.
(19) Arcovito, A.; Lamb, D. C.; Nienhaus, G. U.; Hazemann, J. L.; Benfatto, M.; Della Longa, S. *Biophys. J.* **2005**, *88* (4), 2954–2964.
(20) Pettifer, R. F.; Mathon, O.; Pascarelli, S.; Cooke, M. D.; Gibbs, M. R. J. *Nature (London)* **2005**, *435*, 78–81.
(21) Benfatto, M.; Della Longa, S.; Hatada, K.; Hayakawa, K.; Gawelda, W.; Bressler, C.; Chergui, M. *J. Phys. Chem. B* **2006**, *110* (29), 14035–14039.

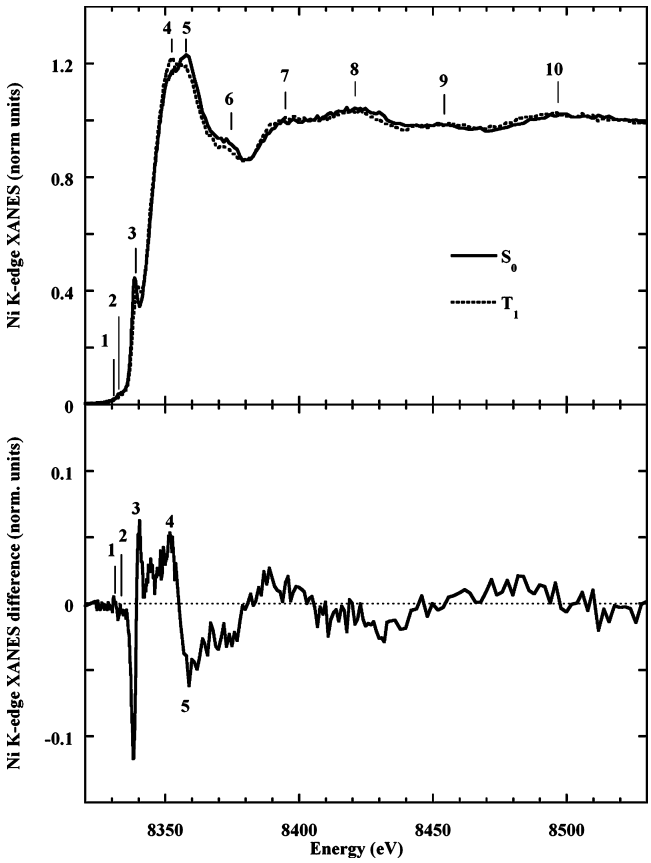

Figure 2. Upper panel: Experimental Ni K-edge XANES spectrum of Ni(II)-TMP of the (solid line) ground state, S_0, and its (dotted line) 100 ps laser-pumped photoproduct, containing about 60% of an excited triplet T_1 state. Lower panel: XANES (pumped minus S_0) difference spectrum of the data reported in the upper panel.

can be successfully applied to time-resolved transient XAS giving a complete local structural characterization for short lifetime transient states.

Methods

Details on the X-ray transient absorption (XTA) experiment with ~100 ps time resolution were reported previously.[1] The Ni(II)TMP photocycle and occupancy of the 3d orbitals has been described by Chen et al.[1] The electronic configuration of Ni(II) ($3d^8$) in the S_0 ground state (nearly square-planar) according to ligand field theory has an empty $3d_{x^2-y^2}$ molecular orbital (MO) and a doubly occupied $3d_{z^2}$ MO. The Q- or B-band excitation induces a $S_0 \rightarrow S_1$ or S $S_0 \rightarrow S_2$ transition. The S_1 or S_2 (π, π^*) state is believed to convert within 350 fs to an intermediate state T_1' that then undergoes vibrational relaxation in less than 20 ps to a relaxed triplet state, T_1, with a presumed $^3(3d_{x^2-y^2}, 3d_{z^2})$ configuration where the $3d_{x^2-y^2}$ and $3d_{z^2}$ MOs are each singly occupied. Finally, the T_1 state returns to the S_0 state in approximately 200 ps.

The excited-state population at a certain time delay after the excitation was evaluated by the time evolution of optical transient spectroscopy. The subpicosecond and <20 ps components were too short to resolve by the nominally X-ray pulses with ~100-ps duration. Hence, a convolution between the excited-state decay kinetics approximated with a single exponential decay profile $A = A_0e^{-t/\tau}$ (where $\tau = 200$ ps is the excited-state delay time constant or the excited-state lifetime) and a Gaussian X-ray pulse profile resulted in a maximum value at a time delay of 80 ps between the two profiles, which is how the time zero in the experiment was chosen with sub-100 ps precision. The average excited-state population at this time delay is 0.37 ± 0.10 assuming that the initial excited-state population A_0 is 0.57 ± 0.10 obtained from an optical transient absorption measurement with a time resolution of 10−15 ps.

Emphasized here is the data acquisition method that allowed intrinsic energy calibration between spectra of the ground state and the laser excited mixture. The energy calibration of the experiment was first carried out extrinsically with a Ni foil standard. Then the energy calibration was also performed intrinsically, by taking the data for the ground and the laser excited states alternately at each data point. This intrinsic energy calibration was accomplished by gating a nine-element solid state germanium detector array (Canberra) after the signals were transformed through the amplifiers and single channel analyzers (SCA). The signals were then connected to two sets of scalers with two gate signals of the same repetition rate as the laser pump pulse at 1 kHz, but at different time delays from the laser excitation. The first time delay coincided with the laser pulse and was used for the spectrum of photoexcited sample. The second time delay was 147.2 μs after the laser pulse and was used for the ground-state spectrum. Hence, any edge energy change from the ground state resulted from the structural change due to the laser excitation rather than from experimental error in energy calibration.

Coordination Models. The effects of porphyrin macrocycle distortions on the XANES spectra were analyzed starting from two idealized porphyrin macrocycle structures, namely, a perfect square-planar conformation and a saddled macrocycle with the metal atom at the saddle point. The coordinates for the former were taken from those of 5,10,14,20-tetramesitylporphyrinato-copper(II) hexachloroantimonate dichloromethane solvate,[22] replacing Cu(II) with Ni(II). The coordinates of the saddled conformation were taken from 2,3,7,8,12,13,17,18-octabromo-5,10,15,20-tetramesityl-porphyrinato-Ni(II).[23] As it will be shown in the Result section, XANES calculations depend weakly on twisting effects, and the fit procedure has been carried out by varying the coordinates of the planar structure only.

XAS Theory and Minimization Procedure. Calculation and fitting of XANES spectra was carried out via the MXAN program,[13] which is based on the full multiple scattering (MS) approach in the framework of the muffin tin (MT) potential approximation. MXAN also takes into account inelastic processes by way of a Lorentzian broadening function.[24,25] The square residual function R_{sq}, and the method used for line-broadening are described in the Supporting Information. A typical shape of the broadening function is depicted in Supporting Information, Figure S1.

The MXAN program has been successfully applied to K-edge spectra of a number of transition metal compounds[14−16,26] and also to interpret XANES spectra taken on hemeproteins in the crystalline state[27,28,18] and in solution.[19] Details of the MXAN analysis applied to differential XANES spectra [photoexcited state minus ground state] of picosecond time-resolved experiments were given

(22) Reed, C. A.; Scheidt, W. R. *J. Am. Chem. Soc.* **1989**, *111*, 6865–6868.
(23) Mandon, D.; Ochsenbein, P.; Fischer, J.; Weiss, R.; Jayaraj, V.; Austin, R. N.; Gold, A.; White, P. S.; Brigaud, O.; Battioni, P.; Mansuy, D. *Inorg. Chem.* **1992**, *31*, 2044–2049.
(24) Muller, J. E.; Jepsen, O.; Wilkins, J. W. *Solid State Commun.* **1982**, *42*, 365–368.
(25) Benfatto, M.; Della Longa, S.; D'Angelo, P. *Phys. Scr.* **2005**, *T115*, 28–30.
(26) D'Angelo, P.; Roscioni, O. M.; Chillemi, G.; Della Longa, S.; Benfatto, M. *J. Am. Chem. Soc.* **2006**, *128* (6), 1853–1858.

previously.[12,19,21] Minimization of the R_{sq} function was performed in [R_1, R_2] parameter space, where $R_1 = d(\text{Ni}-\text{N}_p)$ and $R_2 = d(\text{Ni}-\text{C})$ are the first- and second-shell distances, respectively. An alternative approach was also tested, in which the pyrrole rings of the porphyrin were treated as a perfectly rigid bodies, and fitting procedures were performed in the single parameter space of variable R_1.

The figures of MXAN fitting in the present paper display the theoretical energy scale, in which the zero-energy (the continuum level V_0) corresponds to (8341.9 ± 0.3) eV.

Evaluation of the T_1 Fraction from the MXAN Procedure. The MXAN program calculates the absolute cross section $\sigma_{abs}(E)$ at the X-ray absorption edge for the metal center under study. The cross-section is calculated in Mbarn, corresponding to 10^{-18} cm^2. A proportionality constant A_{norm} is used to scale the calculated $\sigma_{abs}(E)$ to the measured data $\mu_{abs}(E)$. Obviously, the numerical values of $\mu_{abs}(E)$ and A_{norm} can vary depending on metal concentration; however, spectra of $\mu_{abs}(E)$ are given in units where the edge jump is normalized to 1.

To evaluate the T_1 fraction from our XANES difference spectrum, two assumptions have been made: (1) the constant A_{norm} is the same for the spectra of pure S_0 and T_1 states; (2) the difference spectrum results from the transition between only the two states, S_0 and T_1. Assumption 1 is certainly true because the S_0 and T_1 state contributions to the XAS signal are measured in the same sample under the same experimental conditions. Regarding (2), under the conditions of the experiment, the features of the measured XANES difference spectrum will be identical to the spectrum corresponding to 100% T_1 conversion, scaled for the factor x of T_1 fraction. In other words, the difference spectrum [$T_1 - S_0$] corresponding to 100% conversion is

$$\sigma_{T_1}(E) - \sigma_{S_0}(E) = A_{norm}[\mu_{T_1}(E) - \mu_{S_0}(E)]$$

while for a x-fractional conversion to the T_1 state

$$\sigma_{T_1}(E) - \sigma_{S_0}(E) = [(x)A_{norm}\mu_{T_1}(E) + (1-x)A_{norm}\mu_{S_0}(E)] - A_{norm}\mu_{S_0}(E)$$

This equation reduces to

$$\sigma_{T_1}(E) - \sigma_{S_0}(E) = A'_{norm}[\mu_{T_1}(E) - \mu_{S_0}(E)]$$

and

$$A'_{norm} = xA_{norm}$$

where $\sigma_{T_1}(E) - \sigma_{S_0}(E)$ is calculated during the MXAN fit to the experimental difference XAS spectrum. The values of A_{norm} and A'_{norm} are directly extracted from the MXAN procedure when applied to the S_0 absolute spectrum, and to the difference spectrum, respectively, and the A_{norm}/A'_{norm} ratio gives the T_1 fraction "x" without the need for any further information.

Results

Figure 2 displays the experimental Ni K-edge XANES spectra of Ni(II)TMP at its ground state, S_0, and the laser excited mixture taken at nominally 100 ps delay after the laser pump pulse (1 mJ, 5 ps fwhm, 527 nm, and 1 kHz repetition rate), as reported by Chen et al.[1] According to the optical transient absorption measurements, the laser excited mixture has approximately 0.37 ± 0.10 fraction of the excited state, T_1 as described in the Methods section. Weak features **1** (at 8331 eV) and **2** (at 8333.2 eV) are present in the pre-edge region, and are assigned to 1s → 3d transitions that are sensitive to the electronic structural change induced by the laser. The rising edges of the spectra exhibit a distinctive sharp feature **3** (at 8338 eV), which is shifted to 1.5 eV higher in energy in the T_1 state from that of the S_0 state. The origin of such a shift is not completely clear, although the result is consistent with a greater effective nuclear charge, Z_{eff}, of Ni(II) due to the ring expansion observed in the EXAFS spectra.[1] Moreover, significant changes are observed in the "white line" region of 8350−8360 eV (peaks **4** and **5**) and beyond (peaks **6**−**10**), which have been attributed to energy level shifts of $4p_x$ and $4p_y$ MOs convoluted with multiple scattering contributions.[1,29] The energy splitting between peaks **3** and **4**, and between peaks **4** and **5**, are about 14 and 5 eV, respectively. In the lower panel of Figure 2, the XANES difference spectrum of the same states, [photoexcited − S_0], is displayed. By assuming that the observed spectral changes are due to a perfect two-state transition where only a fraction of S_0 converts to the T_1 state, the overall shape of the XANES difference spectrum will be identical to the spectrum corresponding to 100% T_1 conversion, the overall amplitude being given by the T_1 fraction. This correspondence is shown by the simple relation

$$\text{"pumped XAS spectrum"} = x \times T_1 + (1-x)S_0$$

Then the difference spectrum is

$$[\text{"pumped XAS spectrum"} - S_0] = x(S_0 - T_1)$$

where "x" is a fraction that affects intensity only.

XANES Analysis of the S_0 State. Given these experimental results, the XANES spectrum of a ground-state Ni(II)porphyrin cluster was calculated as a function of the cluster size. The calculated XANES spectra corresponding to 1-shell (NiN_4), 2-shell (NiN_4C_{12}), and 3-shell (Ni-porphyrin) clusters are depicted in Figure 3. It is evident that all the experimental features **4** to **10** are well reproduced by the calculations. We note that including three shells is essential for a successful simulation. In Figure 3 inset, a blow-up of the edge features in the 3-shell calculation is displayed. The calculated edge contains a weak shoulder (feature **3′**) that, relative to experimental peak **3**, has a different energy splitting from peak **4** (8.5 instead of 14 eV). Possible explanations of the failure in reproducing peak **3** are given in the discussion section.

MXAN fits to the XANES spectrum of the S_0 ground state were then carried out, with the results given in Figure 4. The S_0 spectrum was fit in the [R_1, R_2] parameter space, where $R_1 = d(\text{Ni}-\text{N}_p)$ and $R_2 = d(\text{Ni}-\text{C})$ are the first shell and second-shell distances, respectively. The third shell

(27) Della Longa, S.; Arcovito, A.; Girasole, M.; Hazemann, J. L.; Benfatto, M. *Phys. Rev. Lett.* **2001**, *87* (15), 155501.
(28) Della Longa, S.; Arcovito, A.; Benfatto, M.; Congiu-Castellano, A.; Girasole, M.; Hazemann, J. L.; Lo Bosco, A. *Biophys. J.* **2003**, *85* (1), 549–558.
(29) Westre, T. E.; Kennepohl, P.; De Witt, J. G.; Hedman, B.; Hodgson, K. O.; Solomon, E. I. *J. Am. Chem. Soc.* **1997**, *119*, 6297–6314.

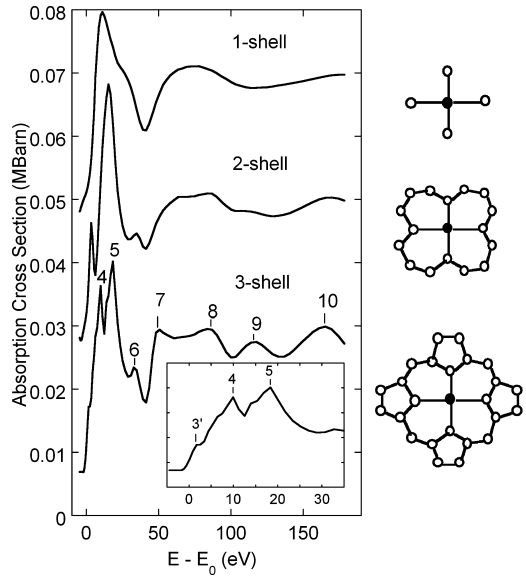

Figure 3. Theoretical XANES spectrum of square planar Ni(II)-porphyrin as a function of the cluster size. The atoms entering the calculation are shown along the right abscissa. The calculations were done without including any damping from inelastic losses, to emphasize the origin of each feature. From these calculations, peaks 4 and 5 (absent in the 1-shell and 2-shell calculations) can be attributed to multiple scattering (MS) signals coming from photoelectron pathways extending over the entire 3-shell cluster.

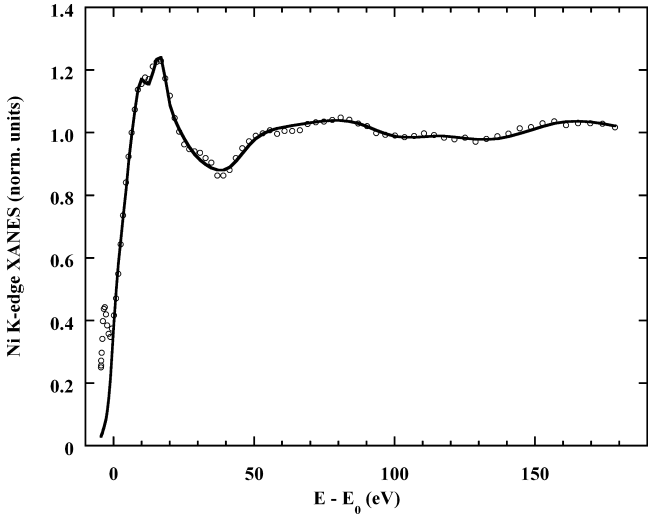

Figure 4. MXAN fit (solid line) of the XANES spectrum of the S_0 ground state (circles). The values $R_1 = d(\text{Fe}-\text{Np}) = (1.93 \pm 0.02)$ Å and $R_2 = d(\text{Fe}-\text{C}) = (2.94 \pm 0.03)$ Å were obtained from the fit.

followed rigidly the second shell distance. The porphyrin was mantained perfectly planar (twisting effects are discussed below), varying the R_1 and R_2 coordinates of the compound of Figure 1A. The starting R_1 distance was 1.91 Å. The resulting absorber-scatterer distances were $R_1 = (1.93 \pm 0.02)$ Å and $R_2 = (2.94 \pm 0.03)$ Å, which are comparable with the crystallographic distances found in the octabromo homologue (1.916 Å and 2.94 Å, respectively)[23] and with EXAFS values.[1] Hence, the utility of MXAN in determining structural parameters of a metalloporphyrin is verified, though the energy range for the fitting is slightly shorter (by about 5−10 eV) than in previous studies on metal ions in water and hemoproteins.[12,19,21] This point is discussed further below. Although peaks **1**, **2**, and **3** were not reproduced, the fit is satisfactory in the energy range from 8341 eV (above peak **3**) to 8550 eV ($k = 7$ Å^{-1}). In addition, the R_1 and R_2 values remain unchanged by including peaks **1**, **2**, and **3** in the fit, but the R_{sq} from the fit increases by about 400% because of the irreproducibility of peak **3**. Thus, these results are clear evidence that the MT approach can be successfully applied to open systems such as square-planar Ni porphyrins, giving an excellent theoretical reproduction of the XAS spectra and quantitative structural recovery.

XANES Analysis of the (Photoexcited − S_0) Difference Spectrum. To obtain the optimized average $d(\text{Ni}-\text{N}_p)$ and $d(\text{Ni}-\text{C})$ of the T_1 excited state, MXAN was used to fit the experimental XANES [photoexcited − S_0] difference spectrum. This analysis is different from the EXAFS analysis performed by Chen et al.[1] which was carried out on a "pure T_1" XAS spectrum reconstructed from the fractional photoconversion evaluated from transient optical spectroscopy. The evaluation made in their work (T_1 fraction = 0.50) has been reconsidered now as 0.37 ± 0.10 taking into account the various sources of uncertainty of that measure. In contrast, as described under Methods, the MXAN analysis reported here allows the normalization constant between the theoretical and experimental difference spectrum to vary as a fitting parameter yielding the T_1 fraction directly. However, by experimental evidence only and under the assumption that a two-state transition occurs, the T_1 fraction must be greater than about 0.35 and lower than about 0.75. The upper limit is obtained under the assumption of 100% T_1 conversion after laser excitation, by convoluting the T_1 decay profile with the 150 ps X-ray pulse width. Moreover if we assume a T_1 fraction <0.35, the reconstructed XANES spectrum of the hypothetical "pure T_1" state displays an impossible negative absorption peak at the rising edge (see Supporting Information and Figure S2).

When considering XANES difference spectra, a shift of the ionization energy between the two photostates can occur, reflecting intramolecular electron transfer processes that alter the net charge of the metal center. This chemical shift is presently not included in the MXAN protocol, but can be entered manually if necessary. Differential XAS analysis is also extremely sensitive to energy calibration of the beamline, which requires very careful confirmation. As stated in the Methods section, an intrinsic energy calibration was implemented in the data acquisition. Therefore, the edge energy differences between S_0 and T_1 states are due to the electronic and structural changes and not to a systematic error.

Results from a set of fit procedures is given in Table 1, each of which differs from others by the choice of structural variables, and the imposed chemical shift. Fits #1−#5 were performed in the two-shell, double variable space [R_1, R_2], while fits #6−#8 were performed in the single variable space $d(\text{Ni}-\text{N}_p)$. For the latter fits, the pyrrole rings were considered perfectly rigid. Single and double parameter space fits were evaluated assuming different chemical shift values ranging from 0.0 to −2.0 eV. Here, the negative sign corresponds to a blue-shift of the XANES spectrum relative to that of S_0, indicating more positive charges on Ni in the T_1 state. This set of choices in chemical shift was made to

Table 1. Summary of Fits of the (Photoproduct-S_0) XANES Difference Spectrum[a]

fit	chemical shift (eV)	T_1 fraction	R_{sq}/n[b]	Δd(Ni−N) R_1 (Å)	Δd(Ni−C) R_2 (Å)	Δd(Ni−pyr) (Å)
ref 1 fit		45−50%		0.08(2)	0.07(2)	
1	0.0	70%	2.14	0.04(2)	0.05(3)	
2	−0.5	54%	2.36	0.06(2)	0.06(3)	
3	−1.0	46%	2.86	0.09(2)	0.08(5)	
4	−1.5	46%	3.57	0.10(2)	0.09(4)	
5	−2.0	41%	4.06	0.13(3)	0.05(4)	
6	0.0	59%	2.56		(0.05)	0.06(2)
7 ESH_fix	0.0	44%	3.45		(0.06)	0.07(2)
8 ESH_fix	−0.5	46%	3.10		(0.07)	0.08(2)

[a] The values found for the fit of the ground state (absolute spectrum) are: d(Ni−N) = R_1 = 1.93 ± 0.02; d(Ni−C) = R_2 = 2.94 ± 0.03. Fits #1−#5 are optimized in the double parameter space [R_1−R_2], fits #6−#8 in the single parameter space d(Ni−pyrrol). Statistical errors are last digits in parentheses. In fits #7 and #8 the parameter "ESH" (used for energy alignment exp. vs. theo.) is restrained to the value found for the fit of the ground state, i.e., 8341.9 ± 0.3. Note that the T_1 fraction is provided by our fit, while the chemical shift is assumed "a priori"; hence, different fits correspond to different choices of the chemical shift. [b] A merit factor Rsq/n is reported here, where n is the number of parameters; it is defined in the Supporting Information.

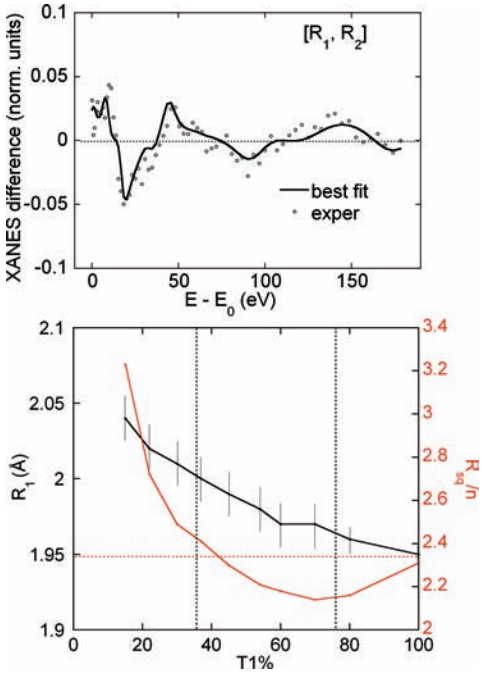

Figure 5. Upper panel: XANES difference spectrum [photoproduct − S_0] (circles) and the MXAN best fit (solid line) giving the optimized average Ni−N and Ni−C distances, and a T_1 fraction of 0.70 Lower panel: Plot of R_1 (black line, including statistical errors) and R_{sq}/n (red line) as a function of the T1 fraction. According to the plotted results, R_1 = (1.98 ± 0.03) Å (ΔR = 0.05 Å) and the T_1 fraction is (0.60 ± 0.15). Evaluations take into account the (0.35−0.75) T_1 fraction limits, and correspond to 10% R_{sq}/n increase around the global minimum.

test whether Z_{eff} of Ni(II) changes in the pumped triplet state.

As expected, the fitting results change systematically with the chemical shift chosen between T_1 and S_0 (Table 1); however, our best fit conditions correspond to a chemical shift of 0.0 eV, indicating no change in Ni(II) Z_{eff} in the triplet state molecule.

A graphical representation of the MXAN analysis in the [R_1, R_2] parameters space is shown in Figure 5, lower panel. The T_1 fraction varies between 0.15 and 1.0, whereas no chemical shift is included here. The values found for R_1 (black points) and the corresponding value of R_{sq}/n (red curve, n is the number of parameters) are depicted. The statistical error on R_1 is also reported. It can be noted that when the chosen T_1 fraction approaches 1.0, this error becomes very small. It is due to the fact that the fit sensitivity is maximum when T_1 fraction = 1.0, whereas the R_1 increase is minimal (0.02 Å). A global minimum is found near 0.70 T_1. In the upper panel the best fit of the XANES difference spectrum at the global minimum is displayed. The R_{sq}/n variation in the range 0.45−0.75 is small, whereas the statistical correlation between the T_1 fraction and R_1 is rather strong, thus no significant difference is obtained with respect to the previous EXAFS result as far as it concerns the R_1 distance elongation. According to the overall set of calculations, R_1 = (1.98 ± 0.03) Å (ΔR = 0.05 Å) and the T_1 fraction is (0.60 ± 0.15). These evaluations are taken within the limits imposed by the experimental evidence (0.35−0.75, dashed vertical lines), as corresponding to 10% R_{sq}/n increase (red dashed line) around the global minimum placed at T_1% = 70%; R_1 = 1.97 Å; with R_{sq}/n = 2.14. The T_1 fraction is different from what was measured by optical transient spectroscopy (0.37 ± 0.10), but the two evaluations are compatible within their respective errors.

This result is obtained by XANES analysis only. On the other hand, by using the independent information from optical spectroscopy (T_1 fraction = 0.37 fourth point plotted) we obtain R_1 = (2.00 ± 0.02) Å (ΔR = 0.07 Å), but the R_{sq}/n increases by about 15%. By assuming a chemical shift of −1.5 eV, the T_1 fraction of the global minimum diminishes (0.30) but the R_1 increase becomes very large (R_1 = 2.05 Å) and square residual increases relevantly (R_{sq}/n = 3.72).

Twisting Effects. The effect of porphyrin macrocycle distortions on the XANES spectra by comparing results from two idealized porphyrin macrocycle structures. The first macrocycle included a perfect square-planar conformation, while the second featured a saddled macrocycle with Ni atom in the saddle point. The two structures are depicted in Figures 1A and 1B. The coordinates for the former were taken from the structure of copper(II)-tetramesitylporphyrin[22] replacing Cu(II) with Ni(II), and coordinates for the saddled conformation were taken from a nickel(II)- tetramesityl-octabromoporphyrin,[23] in which the eight bromine substituents were replaced by hydrogens at 0.959 Å. In the latter reported structure d(Ni−N) has the same value as measured by EXAFS on Ni(II)TMP in toluene solution.[1] The first-shell coordination symmetry in the saddled porphyrin macrocycle deviates from square-planar toward flattened tetrahedral, with trans-N_p−Ni−N_p angle of 170°. The pyrrole rings of the porphyrin macrocycle are further distorted with respect to the xy plane, as well as rotated along the Ni−N_p bond. For a meaningful comparison, the two clusters used in the MS calculations included the same 24 porphyrin atoms (no hydrogens included) and identical line broadening terms.

To separate the effects of macrocycle twisting from those of bond elongation, two MXAN simulations of the saddled-shaped and the square-planar structures were compared, while keeping d(Ni−N) fixed at 1.93 Å (Figure 6, upper panel). Following this, two square-planar structures with d(Ni−N) values, of 1.93 Å and 2.01 Å, were compared

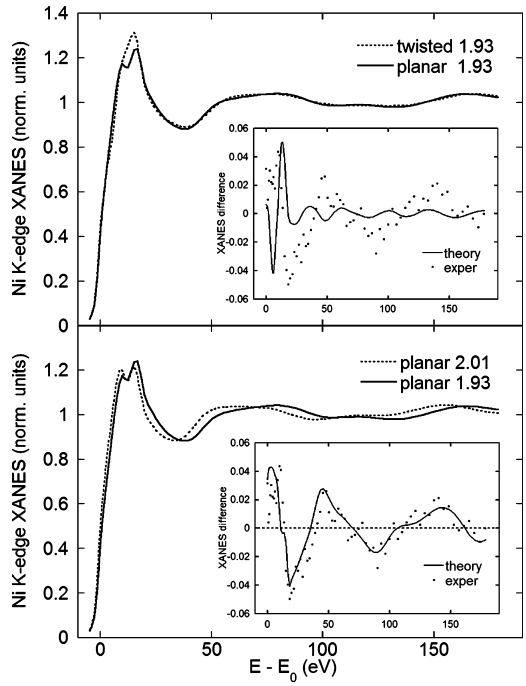

Figure 6. Upper panel: theoretical XANES spectra of structure A (planar, solid line) and structure B (saddle-shaped, dotted line), having the same $d(Ni-N_p)$ distance of 1.93 Å. Lower panel: theoretical XANES spectra of structure A with two different $d(Ni-N_p)$ distances, 1.93 Å (solid line), and 2.01 Å (dotted line). Distance values are reported on the face of the Figure. In the inset of each panel, the calculated difference spectra corresponding to 50% T1 conversion (solid line) are compared with the experimental [photoproduct − S_0] spectrum.

(Figure 6, lower panel). The two insets display a qualitative comparison of the theoretical difference spectra with the experimental one, done by assuming a 0.50 T_1 fraction. The results showed that the porphyrin twisting determines second-order effects on the XANES energy range, relevant changes being restricted to the peaks 4 and 5. This is in line with the set of theoretical calculations shown in Figure 3: peaks 4 and 5 arise only by including the full 3-shell cluster, probing photoelectron pathways delocalized all along the porphyrin plane and being sensitive to its distortions. However, the overall XANES changes observed in the $S_0 \rightarrow T_1$ transition are mainly due to changes of the average Ni−pyrrole distance.

Discussion

Solution Structure of T_1 Ni(II)(TMP). Taking the results of the MXAN fits, the derived model of photoexcited Ni(II)TMP includes elongations of about 0.05 Å for both the Ni−N bond and the Ni−C_α distance, relative to the ground-state molecule. As written in the Results section, the T_1 fraction obtained using the independent MXAN fit procedure (0.60 ± 0.15) is different from what was measured using optical transient spectroscopy (0.37 ± 0.10). However, by considering the respective errors affecting these experiments, the results are not contradictory.

The MXAN procedure is poorly sensitive to twisting of the porphyrin structure toward a saddle shaped one, and a more accurate study of distortion effects by XANES waits for improvements of the actual theoretical approximations. However, examination of structurally known nickel(II) porphyrins,[23,30−32] Table 2, shows a systematic trend in Ni(II)−N and Ni(II)−C_α distances with porphyrin distortion. Known structures of Ni(II) porphyrins are dominated by the saddle distortion, which exhibits the average distances, Ni−N = (1.91 ± 0.02) Å and Ni−C_α = (2.94 ± 0.02) Å for 11 structures (see the Supporting Information). These values are consistent with S_0 Ni(II)TMP, but not with the T_1 metrics.

Table 2. Structural Parameters of Nickel(II) Porphyrins[a]

porphyrin	shape	Ni−N (Å)	Ni−C (Å)	exp. frac.	ref
Ni(II)(DPP)	saddle	1.909	2.935		30
Ni(II)(TPP)	twist	1.931	2.978		31
Ni(II)(P)	planar	1.951	3.001		32
$Ni(II)TMPBr_8$	saddle	1.916	2.940		23
S_0 Ni(II)TMP		1.90 ± 0.02	2.92 ± 0.02	55−50	1
T_1 Ni(II)TMP		1.98 ± 0.02	2.99 ± 0.02	45−50	1
S_0 Ni(II)TMP		1.93 ± 0.02	2.94 ± 0.03	0.40 ± 0.15	this work
T_1 Ni(II)TMP		1.98 ± 0.03	2.99 ± 0.03	0.60 ± 0.15	this work

[a] "DPP" is dodecaphenyl porphyrin; "TPP: is tetraphenylporphyrin, and "P" is porphyrin.

It is also noteworthy that Cu(II)(TMP), which includes a singly populated $3d_{x^2-y^2}$ orbital in analogy to T_1 Ni(II)TMP, also exhibits elongated bond lengths relative to ground-state NiTMP, that is, Cu−N = 2.01 Å and Cu−C_α = 3.03 Å. Likewise, copper(II) porphyrin bond lengths follow a trend of diminishing Cu−N distance with increasing distortion of the porphyrin molecule away from planarity (see in the Supporting Information). Thus, the elongated Cu−N metrics for Cu(II)TMP reflect its planar structure. From these considerations, it seems likely that the porphyrin moiety of T_1 Ni(TMP) significantly distorts away from its ground-state structure upon photoexcitation. This distortion involves elongation of the Ni−N bonds to lengths more consistent with a planar porphyrin. Therefore, we suggest that ground-state (S_0) Ni(II)TMP is approximately saddle-shaped, in analogy to its octabromo analogue. Furthermore, we suggest that photoexcited T_1 Ni(II)TMP, in contrast, is nearly planar. Thus, the relaxation from the initial S_1 photoexcited state to the 100 ps T_1 state is predicted to include a relaxation of a saddle-shaped porphyrin ligand to one that is planar. Therefore, our MXAN results should mean that S_0 (and S_1) NiTMP are saddled porphyrins. The photorelaxation of $S_1 \rightarrow T_1$ NiTMP is accompanied by structural relaxation of a saddle-shaped photoexcited S_1 NiTMP to a planar porphyrin in T_1 NiTMP. The planar porphyrin reflects accommodation of the longer Ni−N bond lengths of T_1 NiTMP. The longer Ni−N bond lengths of the T_1 excited state are induced by new electronic repulsions, which follow from the promotion of the valence photoelectron and the resulting half-filled $3d_{x^2-y^2}$ orbital of photoexcited Ni(II). Thus, the MXAN results combined with chemical reasoning produces a coherent picture of the picosecond structural adjustments made by Ni(II)TMP to accommodate the sudden electronic rearrangements stemming from photoexcitation.

(30) Nurco, D. J.; Medforth, C. J.; Forsyth, T. P.; Olmstead, M. M.; Smith, K. M. *J. Am. Chem. Soc.* **1996**, *118*, 10918–10919.
(31) Maclean, A. L.; Foran, G. J.; Kennedy, F. J.; Turner, P.; Hambley, T. W. *Aust. J. Chem.* **1996**, *49*, 1273–1278.
(32) Jentzen, W.; Turowska-Tyrk, I.; Scheidt, W. R.; Shelnutt, J. A. *Inorg. Chem.* **1996**, *35*, 3559–3567.

Validation of the Muffin Tin Full Multiple Scattering Approach. The results demonstrate that MXAN can extract metrical details of transient excited-state molecules from analysis of pump-probe XAS spectra. The ground state to excited state ratio in the photopumped XAS spectrum can be ascertained without the need for any further information. An excellent simulation of the single-electron features of the XANES spectrum was achieved, and structural recovery was obtained for square planar Ni(II)TMP.

Recently, the Muffin Tin (MT) approximation of the molecular potential has been criticized as the main limitation affecting the analysis of the low energy range of the XAS spectrum,[33] especially concerning metal sites with open-shell electronic configurations such as Ni(II) or Fe(II,III). This claim is normally raised as a generally valid statement, without any discussion or any distinction made among different experimental cases. There is still a need to improve the theory of XANES features at very low energy, mainly in the pre-edge energy region. In principle, a complete theoretical reproduction of the spectrum, leading to a complete description of the electronic/geometric configurations, could be accomplished with various improved approximations.[34,35] Indeed, careful experimental distinctions must be made because it is quite hard to predict the size of the non-MT corrections in practice. Checks can now be easily done within MXAN by optimizing the MT-theoretical corrections in comparison with experimental data. This methodological approach avoids any experimenter a priori biases.

The present work confirms previous studies[16,21,36] on metal clusters, in which the MT approach and the full potential Finite Difference Method (FDM)[33,37] were compared. This comparison demonstrated that the differences following the change from the MT to the FDM potential are small and can be further reduced by a physically constrained choice of the interstitial potential.[25,35,38] In this way a full recovery of the geometrical structure around the absorbing atom can be achieved by quantitative analysis of XANES data under the MT approximation. The MXAN analysis of the above-mentioned systems produced structural parameters in agreement with both EXAFS and crystallographic determination.

Origin of the Lower Rising Edge Feature. The difficulty in finding an MXAN fit that included peak **3** on the rising K-edge of Ni(II)TMP deserves further comment. This feature is also present in the K-edge XAS of some square-planar Ni(II) complexes,[39,40] and it has been assigned to a $1s \rightarrow 4p_z$ transition by polarized XAS studies.[40] As stated in the Results section, the R_1 and R_2 values provided by MXAN for the S_0 state remain unchanged by including peaks **1**, **2**, and **3** in the fit, but R_{sq} increases by about 400% because of the irreproducibility of peak **3**. The result of the fit is shown in Figure 7, upper panel. The lower panel of Figure 7 shows a comparison of the low energy part of experimental and theoretical spectra. The core-hole line-broadening has been removed from the theoretical spectrum to improve the visual resolution of the transitions. A broad feature appears in the calculated spectrum at the right energy position of peak **3** although its intensity is not correct. This problem can be due to the so-called "extended continuum" theoretical scheme[41] used in the MXAN procedure. In this scheme the T matrix normalization is used instead of the more standard K matrix. In this way the same concepts are employed to describe both the continuum and the bound-state transitions within the XAS spectrum. That is, this approach treats bound states as scattering resonances. The whole XAS spectrum over the entire energy

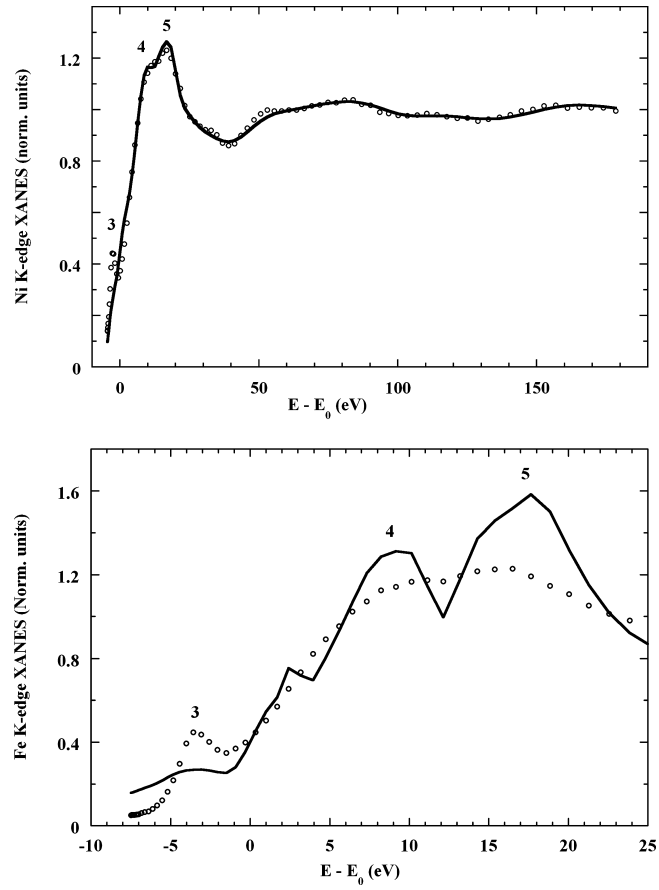

Figure 7. Upper panel: MXAN fit (solid line) of the XANES spectrum of the S_0 ground state (circles) including the lower rising edge in the fit. This fit yielded bond lengths $R_1 = d(\text{Ni}-\text{Np}) = (1.91 \pm 0.02)$ Å and $R_2 = d(\text{Ni}-\text{C}) = (2.96 \pm 0.03)$ Å. Thus, the structural results are identical within errors relative to the fit shown in Figure 4; however, R_{sq} increases by 400% because peak **3** is not well-reproduced. See the text for a discussion of this point. Lower panel: comparison between the experimental S_0 spectrum (circle) and the theoretical best fit (solid line), in the low-energy region. The theoretical calculation did not include experimental line-broadening to emphasize the underlying structure of the transitions. Therefore, the apparent disparity between the calculation and the data arises because broadening by the inelastic losses in the experimental data has been removed from the calculation.

(33) Joly, Y. *Phys. Rev. B* **2001**, *63*, 125120–125129.
(34) Rehr, J. J.; Albers, R. C. *Rev. Mod. Phys.* **2000**, *72*, 621–654.
(35) Natoli, C. R.; Benfatto, M.; Della Longa, S.; Hatada, K. *J. Synchrotron Radiat.* **2003**, *10* (Pt 1), 26–42; X-ray absorption spectroscopy: state-of-the-art analysis.
(36) Sarangi, R.; Benfatto, M.; Hayakawa, K.; Bubacco, L.; Solomon, E. I.; Hodgson, K. O.; Hedman, B. *Inorg. Chem.* **2005**, *44*, 9652–9659.
(37) Joly, Y. *J. Synchrotron Rad.* **2003**, *10*, 58–63.
(38) Benfatto, M.; Della Longa, S.; Natoli, C. R. *J. Synchrotron Radiat.* **2003**, *10* (Pt 1), 51–57.
(39) Scott, R. A. *Physica B* **1989**, *158*, 84–86.
(40) Renner, M. W.; Furenlid, L. R.; Barkigia, K. M.; Fajer, J. *J. Phys. IV* **1996**, *7* (1), 661–662.
(41) Tyson, T. A.; Hodgson, K. O.; Benfatto, M.; Natoli, C. R. *Phys. Rev. B* **1992**, *46*, 5997–6019.

range, starting from the interstitial potential, is described in terms of transitions to continuum states. Under this approach, one single continuum calculation gives all the energy separations between the bound-state features and the continuum features, although the transition amplitudes in the bound-state region might be incorrect because of the different normalization used for bound and continuum states. This is particularly true for transitions to deep bound states, as in the case of Ni(II)TMP, where the energy separation between peaks **3** and **5** is of the order of 20 eV.

To investigate peak **3** further, the state-to-state transition energies between the bound states, which are responsible for the pre-edge and lower rising edge region, were calculated using spin unpolarized self-consistent field (SCF-X_α) theory.[42] The formal valence of each atom was assigned by reference to Clementi−Roetti and/or Herman Skillman tables, and pure D_{4h} symmetry was assumed. Only the first and second shells of Ni(II)TMP were included in this calculation. An X_α MT molecular potential was built up by this approach, and the absorption spectrum of the S_0 structure was calculated. Although this procedure does not allow an iterative fitting, it provides an unambiguous comparison between the calculated SCF-X_α transitions to empty bound states and the calculated pre-edge XANES features. The result of this investigation was that the broad feature in the pre-edge region arises from the cross section polarized along the normal to the porphyrin plane, which is consistent with a dipole transition from 1s to the first empty state of A_{2u} symmetry. This corresponds to the $1s\rightarrow 4p_z$ transition, which is analogous to the previous assignment of a similar feature observed in the K-edge XAS of square planar Cu compounds[43] and is in agreement with the experimental results of the polarized XAS study.[40]

An additional finding of the SCF-X_α calculation was that if the total charge of the cluster and the D_{4h} symmetry are kept fixed, the transition energy $1s\rightarrow A_{2u}$ increases by more than 1 eV between the S_0 and the T_1 state. Thus, the experimentally observed blue-shift of peak **3** seems to depend just on ring expansion. Further work would be necessary to assess if twisting effects could be also associated to energy shifts of this feature, as well as the influence of solvent molecules, and the possibility that this feature includes intensity from a *z*-polarized two-electron shakedown transition.

In conclusion, the present work has demonstrated that the MXAN full multiple scattering muffin-tin approach to XAS difference spectra can successfully derive the structural metrics of short-lived photoexcited molecular transients and can be used also independently from secondary information obtained from difficult transient optical experiments to evaluate the fractional ratios of photoproducts in two-state systems. This capability could help researchers faced with the problem of estimating fractional populations from transient electronic spectra in which the absorption spectrum of the excited state is neither well-understood nor known to be baseline resolved from the ground-state spectrum. These experimental ambiguities can affect the derived ground- and excited-state populations, and thus reduce the precision of the transient-state structural metrics obtained from the XAS spectrum. Thus, the new MXAN method should facilitate time-resolved experiments, providing greater understanding of the relationships between electronic and structural states in transient photoexcited species.

Supporting Information Available: Further details about the MXAN analysis of XANES spectra. This material is available free of charge via the Internet at http://pubs.acs.org.

IC8008943

(42) Pedio, M.; Benfatto, M.; Aminpirooz, S.; Haase, J. *Phys. Rev. B* **1994**, *50*, 6596–6602.
(43) Kau, L.-S.; Spira-Solomon, D. J.; Penner-Hahn, J. E.; Hodgson, K. O.; Solomon, E. I. *J. Am. Chem. Soc.* **1987**, *109*, 6433–6442.